

Dissociative Electron Attachment Cross Sections for Ni(CO)₄, Co(CO)₃NO, Cr(CO)₆

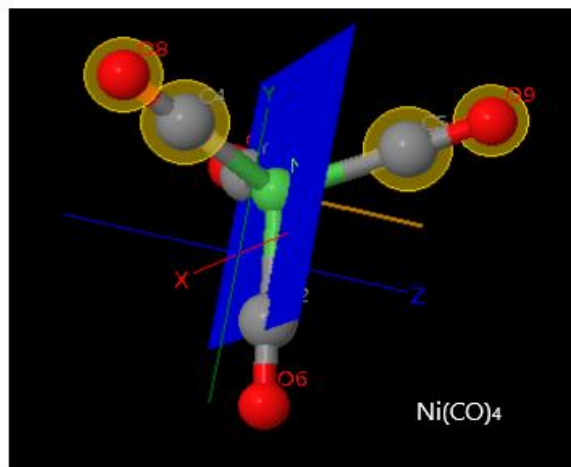
¹Maria Pintea, ¹Nigel Mason, ²Maria Tudorovskaya

¹School of Physical Sciences, University of Kent, CT2 7NZ, Canterbury, UK

²Quantemol Ltd, EC1V 2NZ, London

Abstract

The Ni(CO)₄, Cr(CO)₆, Co(CO)₃NO are some of the most common precursors used for focused electron induced deposition. Some of the compounds, even though extensively used have high requirements when it comes to handling them being, explosives, highly flammable and with high toxicity level, as is the case of Ni(CO)₄. We are employing simulations to determine values that are hard to determine experimentally, and compare them with DFT calculations and experimental data where available.



Using Quantemol-N cross section simulations for dissociative electron attachment (DEA) at low electron energy, 0 – 20eV, gives valuable information on the fragmentation of the molecules, using their bond dissociation energies, electron affinities and incident electron energies. The values obtained for the cross sections are $0.12 \times 10^{-18} \text{cm}^2$ for Ni(CO)₄, $4.5 \times 10^{-16} \text{cm}^2$ for Co(CO)₃NO DEA cross-sections and $4.3 \times 10^{-15} \text{cm}^2$ for Cr(CO)₆.

Introduction

As Focused Electron Beam Induced Deposition^[1] is developing with the possibility of becoming a viable manufacturing technique, the need to have more data available on molecules of interest, alkenes, silanes, metal halogens, carbonyls, phosphines, acetylacetonates,^[1] increases. The limitation of this direct - write fabrication technique comes in the appearance of secondary and backscattered electrons as part of the primary electron beam or secondary electron beam. The effect of the secondary and backscattered electrons at low electron energy level, 0 – 50eV, is the deposition of a thin halo and creation of secondary structures in the vicinity of the primary structures as well as incomplete fragmentation of the precursors

reducing the purity of the final structure. ^[2] To analyze and recreate this effects, gas phase and surface science studies are employed. In gas phase studies, the interaction of molecules with single electrons is evaluated and resulting fragmentation pathways analyzed. On the other hand, in the ultra-high vacuum surface science setups, the interaction of the electrons with the molecules and the substrates is evaluated, identifying the species desorbing from the substrate. However for many of these FEBID compounds, an increase in such information as the probability of collision between electrons and molecules, and the dynamics of the processes underlying the induced chemistry in organometallic compounds is needed and cross sections for: dissociative ionization, elastic scattering, vibrational excitation, dissociative electron attachment, neutral dissociation, bipolar dissociation. The particular metal containing compounds that will be used as the base of our simulations for cross sections determination are compounds that have been extensively researched and used for the deposition purposes and commercially available, but scarce cross section data has been published on them. The data presented from our R-matrix calculations will focus on four widely used compounds $\text{Ni}(\text{CO})_4$, $\text{Co}(\text{CO})_3\text{NO}$ and $\text{Cr}(\text{CO})_6$ commercially available for purchase and widely used in Focused Electron Beam Induced Deposition.

Molecular complexes used for calculations

The carbonyl group compounds ($\text{Ni}(\text{CO})_4$, $\text{Cr}(\text{CO})_6$ and $\text{Co}(\text{CO})_3\text{NO}$) are relatively easy to purchase commercially simple symmetric structures make them suitable for electron-induced chemistry applications and potentially suitable for creating very clean deposits in the focused electron beam induced process with purity over 90% and low resistivity. The structural representation of the three compounds is presented in Fig 2 and the X, Y, Z coordinates used for Quantemol-N calculations are presented in ANNEX 1.

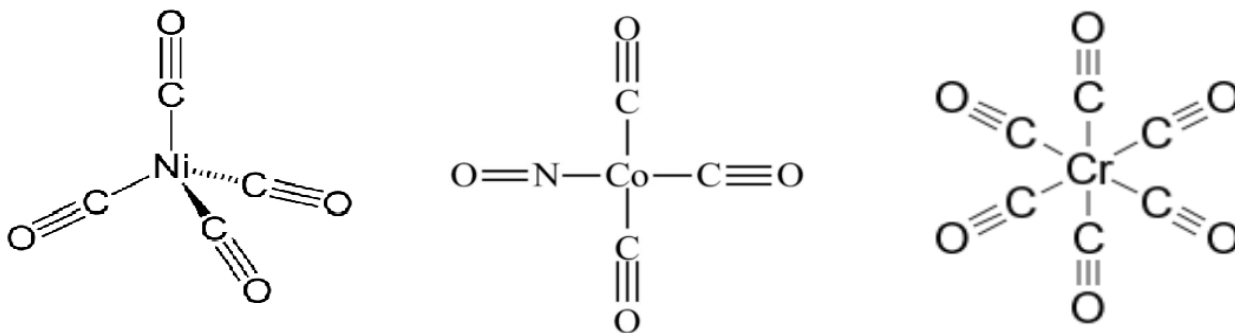


Fig 2. Molecular complexes: $\text{Ni}(\text{CO})_4$, $\text{Co}(\text{CO})_3\text{NO}$ and $\text{Cr}(\text{CO})_6$

The Ni(CO)₄ is less used in the industry due to its high toxicity, similarly to Cr(CO)₆; it is highly flammable and insoluble in water; its lowest decomposition temperature is 50°C, making it hard to be used at room temperature and requiring cryogenic conditions. The Cr(CO)₆ compared to the Ni(CO)₄ has higher volatility and is more stable at room temperature with a thermal decomposition point over 150°C. Similar to the Cr(CO)₆, the Co(CO)₃NO has a high decomposition temperature, 130 – 140°C. Detailed Raman, FTIR and MOs studies are compared in Cross-section section with the theoretical model obtained from our calculations.

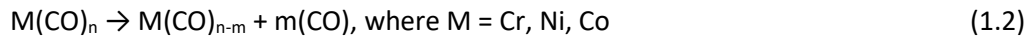
R-matrix theory and method of calculation

Scattering The scattering calculations based on the R-matrix [13] theory are carried out to determine the cross-sections of electron scattering by Ni(CO)₄, Cr(CO)₆ and Co(CO)₃NO. We use Quantemol-N simulation package interfacing UKRmol code suite [52]. Quantemol-N can be used to compute a number of cross-sections for elastic and inelastic electron scattering, the most important to the induced chemistry being the dissociative electron attachment (DEA) cross-sections[15].

The DEA process is a process widely found in nature due to the formation of negative ions at relatively low electron energies, though our applications limit themselves to focused electron beam induced processes. The dissociation process and the induced chemical reactions follow the schematics:



which can be followed by the dissociation reaction:



The DEA process can undertake two paths in the evolution of the compound from gas - phase molecules to fragments or radicals: the first path (a) is the irradiation of the molecule with an electron that would cause a change in the molecule's energy found in a certain resonant state, undergoing a jump to a higher ionized state, and the second path (b) is either a repeated autoionization or if the resonance state has a longer lifetime, dissociation of the molecule into fragments.

The total dissociative attachment cross section is is a weighted sum of DEA cross-sections, σ_i , over all resonances in the scattering process (1.3):

$$\sigma_T(E) = C \sum_i S_i \sigma_i(E) \quad (1.3)$$

The positions of the resonances found with the UKRmol routine RESON [53]. S is the survival probability for the resonance or the probability of a resonance, E is the incident electron energy, and C is the adjustment factor[15]. It is important to note that in the model used by Quantemol-N, the fragments are moving in the effective potential and therefore behave like a quasi-diatomic molecule. For each resonance, the partial cross-section has the Breit-Wigner shape:

$$\sigma_{\text{BW}}(E, r) = (2\pi/E) (\Gamma^2/4) / [(E-V(r))^2 (\Gamma^2/4)] \quad (1.7)$$

where Γ is the width of the resonance, r is the distance between the dissociating fragments, and $V(r)$ is the effective potential.

The resonances positions and widths are determined by the UKRmol codes which treat the incoming electron in the same way as the molecule's electrons in its vicinity inside of the so-called R-matrix sphere. The scattering wavefunction can be expanded over the target states and expressed in terms of N-electron target wavefunctions, continuum orbitals representing the scattering electron inside the R-matrix sphere, and additional quadratic integrable functions constructed from the target occupied and virtual molecular orbitals [13]. Far away from the molecule, the scattered electron moves in the effective potential.

Whilst the *ab initio* part of the calculation is quite rigorous, further assumptions about the dissociation channels and assigning resonances to a specific channel may introduce uncertainty.

The cross section values from Quantemol-N software are in very good agreement with the experimental data available for the particular molecules. In preparing the present calculations we benchmarked the current calculations producing a set of CH₄ cross section data, we obtained the same results for the total cross section and inelastic cross sections, which in previous Quantemol calculations replicated experimental data.

Cross Sections

Co(CO)₃NO. The Co(CO)₃NO compound has C_{3v} symmetry, with the three CO groups on the faces of a tetrahedron and the NO group to Co(IV). The total cross section is high with values of 1.4 x 10⁻¹² cm² for an energy range of 0 - 100eV. Engmann et al (2013) measured the DEA cross section estimating the maximum DEA cross section having a value of 4.1 x 10⁻¹⁶ cm² for the loss of only one CO ligand this being the predominant DEA process and the DI cross sections with values of 4.6 x 10⁻¹⁶ cm².

| Compound | Dissociation | BDE (kcal/mol) |
|------------------------|--------------------------|---|
| Co(CO) ₃ NO | Co + 3CO + NO | 144.8 – 154.4 ^[16] |
| Ni(CO) ₄ | Ni(CO) ₃ + CO | 35 ^[21] , 22.3 ^[44] |
| Co(CO) ₃ NO | Co(CO)+2CO+NO | 115 ^[16] |
| Cr(CO) ₆ | Cr(CO) ₅ + CO | 49.8 ^[26] , 38 ^[25] |

Table 1. Bond dissociation energies for Co(CO)₃NO, Ni(CO)₄, W(CO)₆

The spectroscopy of Co(CO)₃N¹⁵O and Co(CO)₃N¹⁴O in vapor form has been analyzed ^[6], with the infrared spectrum giving vibrational band frequencies at 2108cm⁻¹, 2047cm⁻¹, 1822cm⁻¹ for C - O and N - O stretch and 2010cm⁻¹ for C¹³ - O isotopic species of Co(CO)₂(C¹³O)NO. Bartz et al (1998) determined the highest excited state of Co(CO)₃NO γ₂F_{5/2} at 36300cm⁻¹ equivalent to 103.8 kcal/mol, the three Co - CO bonds and one Co - NO bond needing an extra energy of 154.4 kcal/mol to break the ligands and 38 kcal/mol as the adiabatic metal - ligand bond dissociation energy for two CO groups.

At higher energy, the study of Rosenberg et al (2013) splits the problem in two parts, for irradiation with electron densities less than 5 x 10¹⁶ e⁻/cm² where the C(1s) peaks appear at 287.8eV and 293.3eV, a π-π* transition, the N(1s) that has the peak at 401.6eV, the O(1s) peaks at 534.0eV and 534.6eV and an oxide peak at 529.7eV, and the Co(2p_{3/2}) peak at 780.9eV. For electron densities over 5 x 10¹⁶ e⁻/cm², the C(1s) peak appears only at 285eV, the N(1s) peak does not change its position, the O(1s) peaks attenuate in amplitude and the oxide peak at 529.7eV now increases in amplitude. If the concentration ratios of after and before irradiation are taken into account, a decrease in the values of O/O₀ and C/C₀ is observed and N/N₀ remains constant. The same study presents a reflection absorption infrared spectroscopy study (RAIRs) of the Co - CO and Co - NO bonds, as appearing at 2111cm⁻¹ and 2064cm⁻¹, and respectively 1827cm⁻¹. Comparatively different studies present these vibrational frequencies at 2108cm⁻¹ and 2047cm⁻¹, and NO stretch frequencies at 1822cm⁻¹ (McDowell et al (1961)), and 2100.3cm⁻¹ and 2033cm⁻¹, respectively Co - NO vibrational frequencies at 1806.2cm⁻¹ (Horrocks et al (1963)).

Sawyer et al (2008) determine experimentally the vibrational frequencies at photoinduced dissociation through DFT calculations and picosecond time-resolved infrared spectroscopy showing two bands between 200nm and 400nm. Two types of possible geometries are analyzed, the linear Co - N - O and 120 - 170° angle geometry for the Co - NO bond, giving the vibrational frequency bands for Co - NO at 1808cm⁻¹ in close agreement with the experimental value of 1842cm⁻¹, 1684cm⁻¹ and 1715cm⁻¹. The CO stretching mode appears at 2037cm⁻¹ and 1980cm⁻¹ ^[17]. The presence of the same bent Co - N - O excited state is demonstrated by the anisotropic angular distribution ^[18].

The DEA process is presented in showing the sequential nature of the fragmentation (1.9):

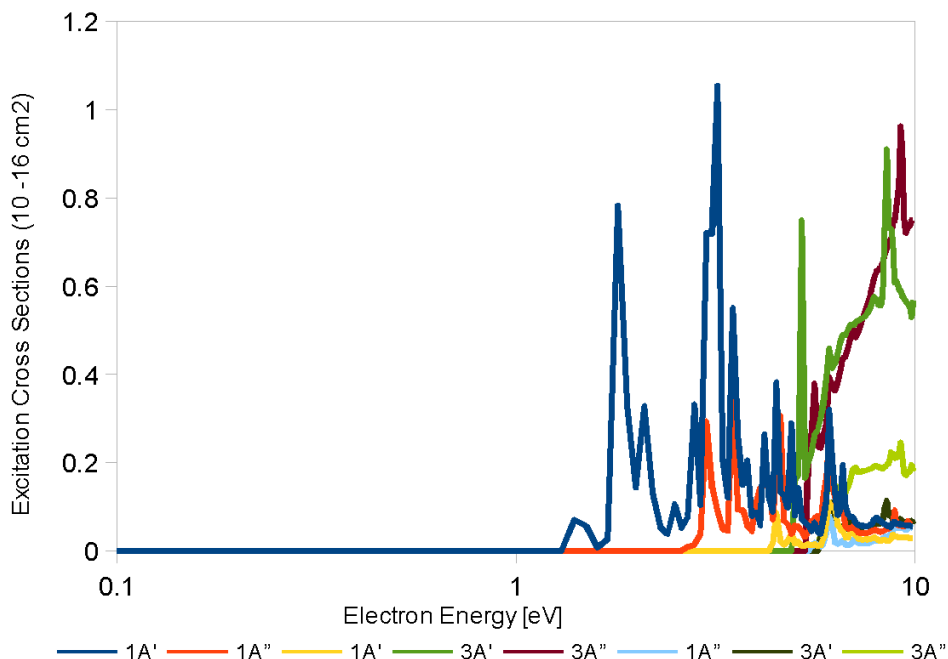
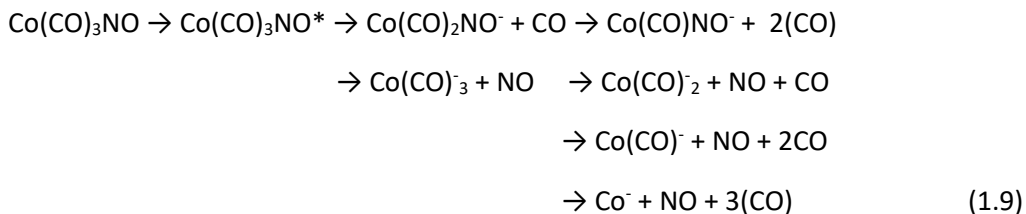


Fig 3. Inelastic Scattering Cross Sections for $\text{Co(CO)}_3\text{NO}$ from Quantemol-N simulations

Knowing that the dissociative electron attachment process happens in the range of 0-15eV (see Table 2), the negative ions are formed at incident electron energies of 0.2eV to 7.1eV, all relatively low electron energies with values under 10eV. The formation of pure Co^- takes place at 7.1eV, stripping off a $(\text{CO})_3\text{NO}$ radical. The dissociative electron attachment to $\text{Co(CO)}_3\text{NO}$ for the dissociation of one CO ligand at 0.9eV with the formation of $\text{Co(CO)}_2\text{NO}^-$ ion is presented in Fig. 3 with values of $\sim 22.5\text{\AA}$. The incident bond dissociation energy for the formation of all negative ions used in our calculations is presented in Table 2.

The $\text{Co(CO)}_3\text{NO}$ has 84 electrons and its ground state is a closed shell 1A_1 state with C_{3v} symmetry and C_1 work point group with its lowest lying excited state 3A . The Co - NO is at 160.8° and Co - N - O is $4A''$ state at 149.5° . With the two bond dissociation energies, for Co - NO bond at a value of 1.63eV and for the Co - CO bond at 1.26eV ^[45], the initial ground state in the fragmentation of $\text{Co(CO)}_3\text{NO}$ is $^3A''$ with the excitation states $^1A'$, $^1A''$, $^1A'$, $^3A'$, $^3A''$, $^1A''$, $^3A'$, and the $^3A''$ giving the symmetry scattering resonances from

the triplet state as $^2A'$, $^2A''$, $^4A'$ and $^4A''$. To simplify our Quantemol-N simulations, a C_{2h} geometry of the molecule was used. The active space from the Quantmeol-N simulation is $29A'$, $30A'$, $13A''$, $14A''$.

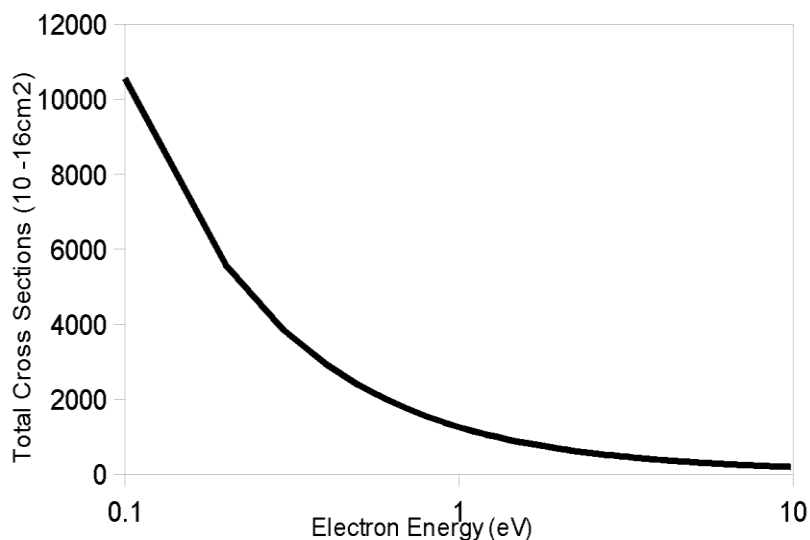


Fig 4. $\text{Co}(\text{CO})_3\text{NO}$ total cross sections from Quantemol-N

The ionization energy for the $\text{Co}(\text{CO})_3\text{NO}$ has a value of 8.33eV for an electron affinity of 0.75eV, with the ionization threshold at a value of 9.2eV. The presented reaction energy for the dissociation of the $\text{Co}(\text{CO})_3\text{NO}$ into $\text{Co}(\text{CO})_2\text{NO}^- + \text{CO}$ is in the range of 0.65eV.

| Negative Ion | Incident Electron Energy (eV) ^[7] | Ion Formation | Incident Electron Energy (eV) ^[41] | Negative Ion | Incident Electron Energy (eV) ^[32] |
|-------------------------------------|--|----------------------------|---|----------------------------|---|
| $\text{Co}(\text{CO})_2\text{NO}^-$ | 0.9 | $\text{Ni}(\text{CO})_3^-$ | 0.8 | $\text{Cr}(\text{CO})_5^-$ | 0.1 |
| CoCONO^- | 2 | $\text{Ni}(\text{CO})_2^-$ | 1.7 | $\text{Cr}(\text{CO})_4^-$ | 1.5 |
| CoNO^- | 5 | $\text{Ni}(\text{CO})^-$ | 4.6 | $\text{Cr}(\text{CO})_3^-$ | 4.7 |
| $\text{Co}(\text{CO})_3^-$ | 1.8 | Ni^- | 5.4 | $\text{Cr}(\text{CO})_2^-$ | 5.9 |
| $\text{Co}(\text{CO})_2^-$ | 3 | | | CrCO^- | 8.5 |
| CoCO^- | 6.4 | | | Cr^- | 8.8 |
| Co^- | 7.1 | | | | |

Table 2. Negative Ion Formation for $\text{Co}(\text{CO})_3\text{NO}$, $\text{Ni}(\text{CO})_4$ and $\text{Cr}(\text{CO})_6$

The dissociative electron attachment cross section for $\text{Co}(\text{CO})_3\text{NO}$ is presented according to the electron affinity, bond dissociation energy and incident electron energy. The electron affinity of the negative ions formed through the dissociative electron attachment process are discussed in ^[27] with values close to

$1.35\text{eV} < \text{EA}[\text{Co}(\text{CO})_2^-] < \text{EA}[\text{Co}(\text{CO})(\text{NO})^-] < \text{EA}[\text{Co}(\text{CO})_3^-] < \text{EA}[\text{Co}(\text{CO})_2\text{NO}^-] = 1.73\text{eV}$. The simulations were run taking into account these differences.

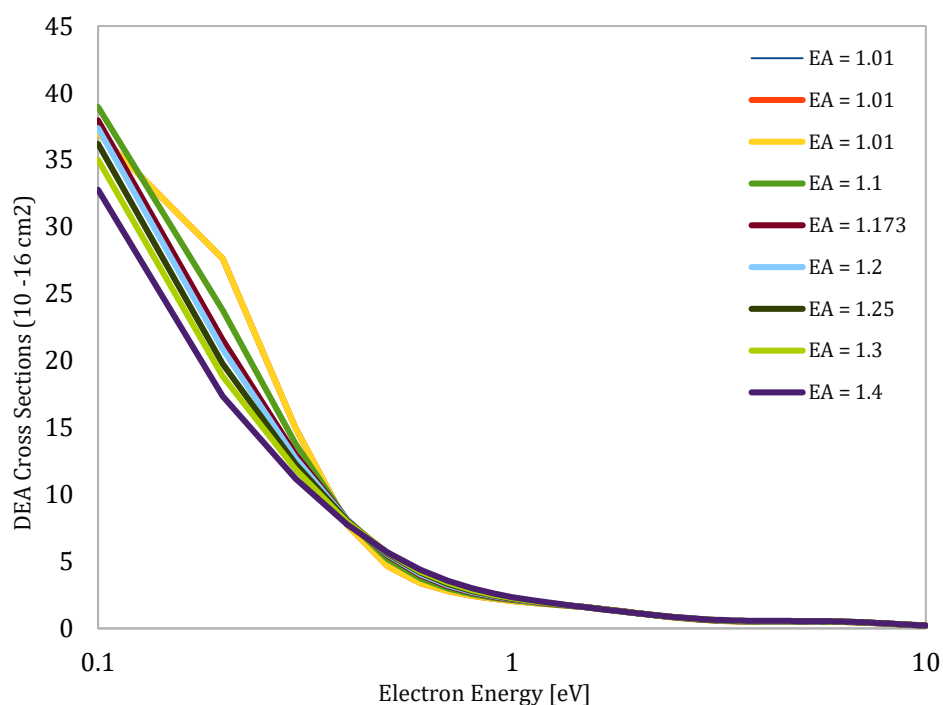


Fig 5. Dissociative electron attachment cross sections from $\text{Co}(\text{CO})_3\text{NO}$

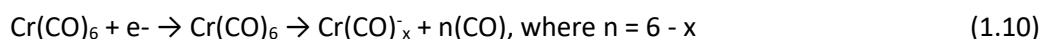
The maximum of the cross section is in the range of $4.5 \times 10^{-16}\text{cm}^2$ at 0.1eV corresponding to the $\text{Co}(\text{CO})_2\text{NO}^-$ fragment.. The individual peaks in the DEA cross section graph are corresponding to the individual fragment dissociation, close in energy to the eV value we found in the literature, though the individual cross section values are very low compared to the computed $\sim 0\text{eV}$ value. The maximum cross section value changes with the vibrational frequency. The purple (color) (Fig. 3) curve is close to reality, presenting a clean peak at a vibrational frequency of 0.53\AA^2 and 1.173eV electron affinity.

$\text{Cr}(\text{CO})_6$. The $\text{Cr}(\text{CO})_6$ bond distances we used for our simulations are 1.916\AA between $\text{Cr} - \text{C}$ and 1.171\AA between $\text{C} - \text{O}$ and the symmetry point group of the ground state molecules is O_h , though different sets of values have been reported in ^[50]. The bond distances reported in $\text{Cr}(\text{CO})_6$ are 1.926\AA for in axis $\text{Cr} - \text{C}$ and 1.139\AA for $\text{C} - \text{O}$. The values are reduced for the equatorial bonds for $\text{Cr} - \text{C}$ with a value of 1.918\AA and $\text{C} - \text{O}$ with a value of 1.141\AA .^[50] This values have been used for the structure of the $\text{Cr}(\text{CO})_6$ in our Quantemol-N calculations. The symmetry point group of the molecule is O_h , but for our simulations simplification we used a D_{2h} configuration.

| Molecule | Bond distances (Å) CCSD (Cr – C) ^[51] | Bond distances (Å) CCSD (C – O) ^[51] | Bond distances (Å) CCSD (Cr – C) _{eq} ^[50] | Bond distances (Å) CCSD (C – O) _{eq} ^[50] |
|---------------------|---|--|---|--|
| Cr(CO) ₆ | 3.684 | 2.207 | 1.918 | 1.141 |

Table 3. Bond distances for Cr(CO)₆

The structural and symmetry data used is presented in Annex 1. Whitaker and Jefferey ^[28] determined the space group of Cr(CO)₆ as the *Pnma* or *Pn2₁a*. The dissociation process in Cr(CO)₆ is following the steps:



The dissociation of Cr(CO)₆ into Cr(CO)₅⁻ and a (CO) radical at 0.1eV, as a result of the dissociative electron attachment (DEA) process, is a transition from the lowest lying LUMO orbital 9a_{1g} (σ) or one of the higher lying virtual orbitals (π) to a HOMO higher energy state orbital (σ*) or to the highest unoccupied HOMO orbital (π*).

The optical spectra of Cr(CO)₆ presents the only one allowed spin transitions ¹A_{1g} → ¹T_{1u} as well as multiple other smaller bands assigned to ¹A_{1g}(2t_{2g}⁶) → ¹T_{1g}, ¹T_{2g}(2t_{2g}⁵6e_{1g}¹) transitions. ^[29], ^[35] The 3.5eV to 7eV was assigned ^[29] to ¹A_{1g} → ¹T_{1u}, while the 4.83eV was assigned to ¹T_{2g} and 4.91eV to ¹A_{1g} → a¹T_{2g}, 3.60eV and 3.91eV was assigned to the allowed transition ¹A_{1g} → a³T_{1u}. Our ions fall in the energy range between 0.1eV to 8.8eV.

| Compound | Fukuda et al ^[36] | Winters and Kiser ^[37] | Foffani et al ^[38] | Electron Ionization ^[11] | Photon Impact ^[11] | Metal Atom ^[11] | Junk and Svec ^[11] |
|---------------------|------------------------------|-----------------------------------|-------------------------------|-------------------------------------|-------------------------------|----------------------------|-------------------------------|
| Cr(CO) ₆ | 8.5 | 8.15 ± 0.17 | 8.18 ± 0.07 | 8.23 | 8.03 | 6.76 | 8.44 ± 0.05 |

Table 3. Ionization potential of Cr(CO)₆

Villaume et al ^[31] defines the structure of the molecule as D_{2h} and the electronic ground state ¹A_{1g} as having the electronic configuration (8a_{1g})²(7t_{1u})⁶(1t_{2g})⁶(1t_{2u})⁶(1t_{1g})⁶(5e_g)⁴(8t_{1u})⁶(2t_{2g})⁶. At 4.48eV and 4.50eV, the allowed transition is a ¹A_{1g} → ¹T_{2u}. At a temperature of 77K, vibrational bands appear at 4.05eV, 4.49eV; at 300K the vibrational bands can be found at 5.53eV, 4.87eV and 6.36eV, all assigned to a¹A_{1g} → ¹T_{1g} and a¹A_{1g} → ¹T_{2g}.

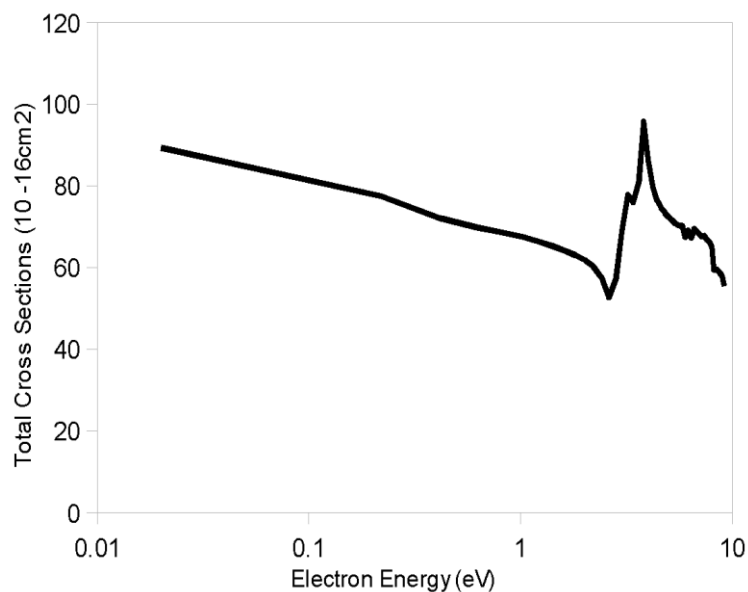


Fig 6. $\text{Cr}(\text{CO})_6$ total cross sections from Quantemol-N

| Negative Ion | Dissociation mechanism (eV) from $\text{Cr}(\text{CO})_6^*$ | Experimental Incident Electron Energy (eV) ^[32] | Electron Affinity (eV) | Vibrational Frequency (cm^{-1}) |
|----------------------------|---|--|---------------------------------|--|
| $\text{Cr}(\text{CO})_5^-$ | $\text{Cr}(\text{CO})_5^- + \text{CO}$ | 0.1 | $>1.6\text{eV}$ ^[38] | 2000 |
| $\text{Cr}(\text{CO})_4^-$ | $\text{Cr}(\text{CO})_4^- + 2(\text{CO})$ | 1.5 | | |
| $\text{Cr}(\text{CO})_3^-$ | $\text{Cr}(\text{CO})_3^- + 3(\text{CO})$ | 4.7 | | |
| $\text{Cr}(\text{CO})_2^-$ | $\text{Cr}(\text{CO})_2^- + 4(\text{CO})$ | 5.9 | | |
| CrCO^- | $\text{Cr}(\text{CO})^- + 5(\text{CO})$ | 8.5 | | |
| Cr^- | $\text{Cr}^- + 6(\text{CO})$ | 8.8 | | |

Table 4. Negative ions of $\text{Cr}(\text{CO})_6$ with electron affinity

The ionization potential for the ions of the $\text{Cr}(\text{CO})_6$ molecule have values higher than the threshold value of $\sim 8\text{eV}$. Table 3 presents the ionization potential of the parent $\text{Cr}(\text{CO})_6$ molecule from the publications of Winters and Kiser ^[37], Fukuda et al ^[36], Foffani et al ^[38] showing a ionization potential for carbonyls with a value of 1.5eV higher than for the metal atom and similar values within $0.1 - 0.5\text{eV}$.

The basis set used for our Quantemol-N calculations on cross sections are cc-pVDZ for C atom, 6-311G for O atom and cc-pVTZ on Cr .

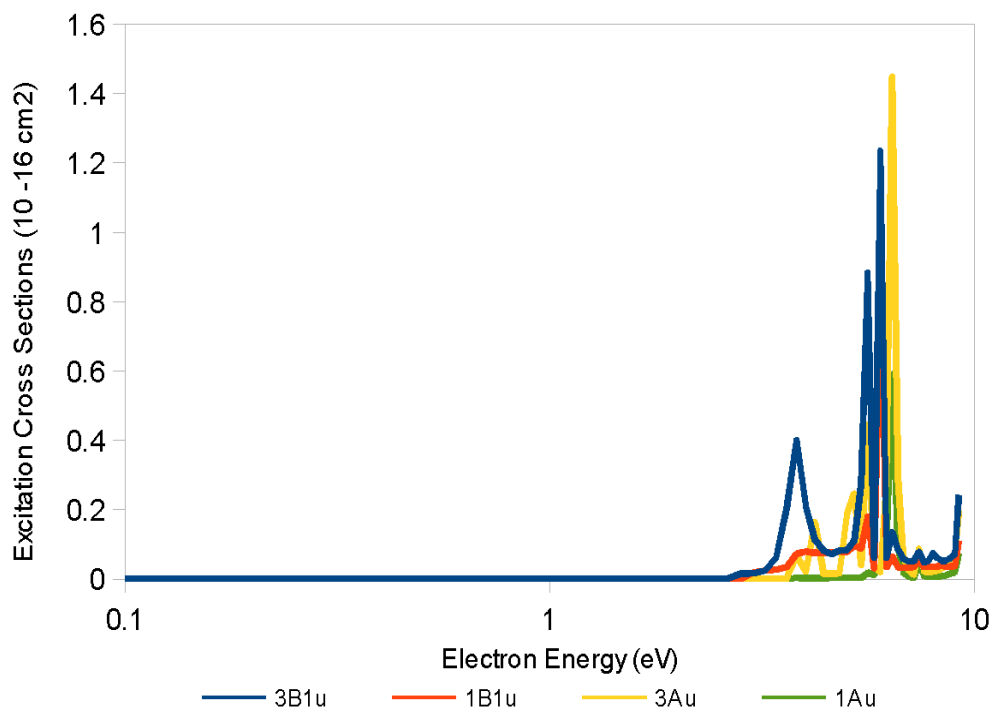


Fig 7. Excitation cross sections of $\text{Cr}(\text{CO})_6$

The DFT calculations in ^[33] reveal the vibrational excitation bands due to the photoionization of the molecule and show the process as being a transition from d_{eg}^* orbitals in σ -antibonding with the metal and a reduction in the number of electrons in π -bonding t_{2g} orbitals to occupying the $\text{Cr-dz}^2 - \text{CO-5}\sigma$ e_g^* orbitals. The cross section data was calculated using Quantemol - N simulations using dissociation electron energy data and electron affinity of the formed negative ions presented in Table 4.

| State | TDDFT/B3LYP - $\Delta E(\text{eV})^{[50]}$ | Experimental ^[50] $\Delta E(\text{eV})$ | Experimental ^[32] / Our Q-N* Sim. $\Delta E(\text{eV})$ |
|-------------------------------|--|--|--|
| 1^1E_u | 4.14 | | |
| 1^1T_{2u} | 4.2 | | |
| 1^1A_{2u} | 4.25 | | |
| 1^1T_{1u} | 4.5 | 4.44 | 4.7 |
| 1^1T_{1g} | 4.65 | | |
| 1^1A_{1u} | 4.7 | | |
| 2^1T_{2u} | 4.82 | | |
| 2^1E_u | 4.71 | | |
| 1^1E_g | 4.99 | | |
| 1^1T_{2g} | 4.74 | | |
| 2^1T_{1g} | 4.91 | | |

| | | | |
|-------------|-------------|-------------|------------|
| 2^1T_{2g} | 5.59 | | |
| 2^1T_{1u} | 6.02 | 5.48 | 5.9 |

Table 5. Vibrational excitation energies of $\text{Cr}(\text{CO})_6$; (Q-N* used for Quantemol-N simulations)

If the $\text{Cr}(\text{CO})_6$ molecule is seen in C_{2v} point group^[50], the allowed transition from 1^1A_1 happens to T_{2u} state that is characterized by 3 sub-states: 1^1B_1 , 1^1B_2 and 2^1A_1 , where 1^1B_1 and 1^1B_2 are degenerate states corresponding to 1^1E in a C_{4v} point group. A Cr – C bond distance higher than 0.25\AA the energy levels of the transition states are: $E(1^1B_1) = E(1^1B_2) > E(1^1A_2)$ for C_{2v} point group and $E(1^1E) < E(1^1B_2)$ for C_{4v} point group. The vibrational and transition states data is presented in Table 5.

The DEA cross sections are presented in Fig. 3, simulated with different electron affinity for comparison in the spectrum changes. The values used for the electron affinity of the negative ions of $\text{Cr}(\text{CO})_6$ are expected to be higher than the specified value in^[38] of 1.6eV. The DEA cross section maximum value is in the range of $\sim 4.3 \times 10^{-15}\text{cm}^2$ at 0.2eV for the $\text{Cr}(\text{CO})_5^-$ fragment, for a value of electron affinity of 1.6 eV and vibrational frequency of 2000 cm^{-1} for a dissociation electron energy value of 0.1eV. The value of cross-sections reported by^[50] is of 1.85\AA^2 to 3.29\AA^2 .

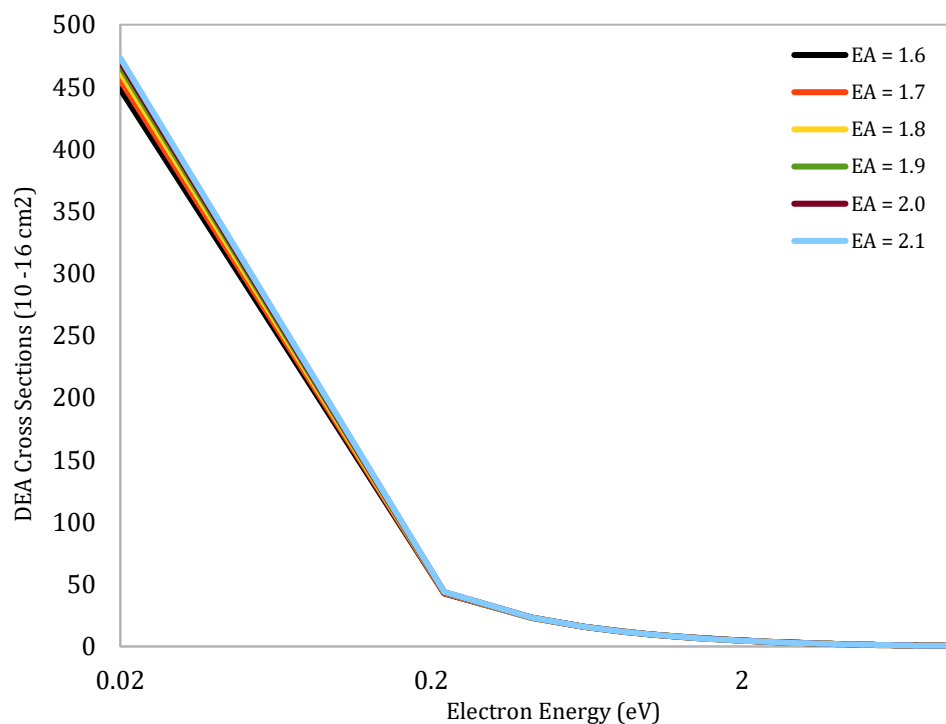


Fig 8. DEA cross sections of $\text{Cr}(\text{CO})_6$

The ground state configuration used in our Quantemol-N calculations in 1A_1 state is D_{2h} . The final assigned states for the DEA process as a result of the calculations from the initial 1A_g state are: $^3B_{1u}$, $^1B_{1u}$, 3A_u , 1A_u with 5 symmetry states. From Quantemol-N simulations we get the resonances from our active space are: 2A_g (4.86eV), $^2B_{3u}$ (9.04eV), $^2B_{2u}$ (9.04eV), $^2B_{1g}$ (8.1eV), $^2B_{1u}$ (8.1eV), $^2B_{2g}$ (8.3eV), $^2B_{3g}$ (8.3eV) and 2A_u (6.7eV).

Ni(CO)₄. The Ni(CO)₄ is a tetrahedral, D_h , with its ground state 1A_1 . The Ni - n(CO) bond is a $d \rightarrow \pi^*$ transition, from the lower stable orbitals d orbitals with ground state (1A_1) to the higher π^* orbitals of t-symmetry with the (1^1T_1 , 1^1T_1 , 3^1T_1 , 1^1E , 2^1T_2) excited states. [20] The UV spectrum of Ni(CO)₄ in [30] has peaks at 6.0eV, 5.4eV and 4.6eV, representing transition dominated by $d \rightarrow 2\pi^*$ for 6.0eV, $^1A_1 \rightarrow ^5T_2$ for 5.36eV close to the 5.4eV value, representing a $d \rightarrow \pi^*$ transition. From 3.36eV to 3.94eV, the transition spectrum is dominated by $d \rightarrow \pi^*$, (A_1 , E, T_1 , T_2) to (T_1 , T_2). The absorption cross-sections value for Ni(CO)₄ is in the range of $\sim 5.01 \times 10^{-17} \text{cm}^2$.

For Ni(CO)₄, the dissociation process follows the reaction equation:

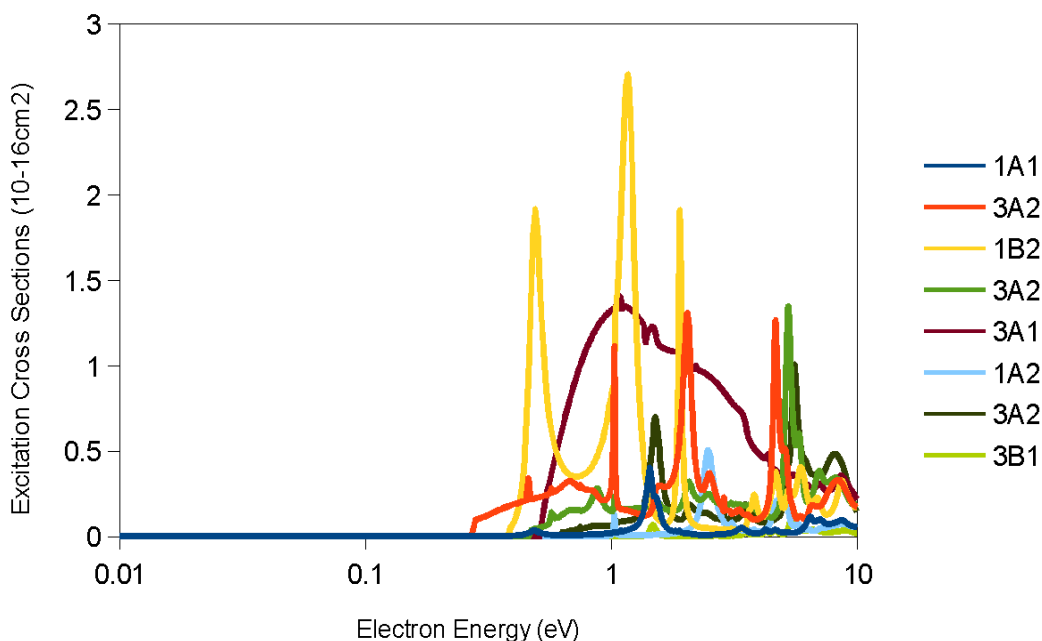
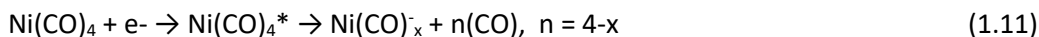


Fig 9. Excitation cross sections of Ni(CO)₄

The Ni(CO)₄ it is known to strip all four ligands in the process of electron-molecule collision, specific to DEA, so we expect to see all the resonances specific to the molecule undergoing full dissociation, with the

negative ions, $\text{Ni}(\text{CO})_3^-$, $\text{Ni}(\text{CO})_2^-$, NiCO^- and Ni^- , at energies between 0.5 – 6eV. As one electron hits one molecule in ground state d and excites it to a higher excited state π^* followed by fragmentation, undergoing an allowed transition, the kinetic energy of the molecule increases from E_G to E_G' to drop further to E_{KER}' and $E_{\text{KER}}'' > E_G$, as we take the fragmentation process as a step by step process. The active space configuration of the theoretical model from our Quantemol calculations is $10A_g, 11A_g, 12A_g, 10A_u, 11A_u, 10B_u, 11B_u, 12B_u, 11B_g$.

The molecular structure with symmetry in Cartesian coordinates (X, Y, Z) used for the cross section simulation parameters is presented in ANNEX 1. As well, the bond distances between Ni - C and C - O have been reviewed from multiple sources, in ^[42] has the values of 1.669Å for Ni – C and 1.153Å for C – O. The bond distances determined in ^[20] experimentally and through calculations have the value of 1.838Å for Ni – C and 1.142Å for C – O from experiment ^[43] and 1.831Å for Ni – C and 1.147Å for C – O determined by CCSD calculations using cc - pVTZ basis set. In ^[46] the Ni - C and C - O bond lengths have a value of 1.84Å and 1.15Å from X-ray single crystal study, and 1.835Å and respectively 1.139Å from gas-phase electron diffraction.

A C_{2h} geometry was employed trying to reduce the calculations steps and the number of iterations. Our Quantemol-N simulations are using a user defined basis set, based on cc-pVTZ and STO-6G. The basis set was user defined to reduce the size of the data and the memory necessary for the simulations.

The values of electron affinity of $\text{Ni}(\text{CO})_4$ used for simulation are presented in Table 6.

| Negative Ion | Incident Electron Energy (eV) ^[41] | Appearance Potentials (eV) ^[40] | Electron Affinity (eV) ^[40] | Vibrational Frequency (cm^{-1}) ^[40] |
|----------------------------|---|--|--|--|
| $\text{Ni}(\text{CO})_3^-$ | 0.8 | 0 | 0.804 ± 0.012 | 2100 ± 80 |
| $\text{Ni}(\text{CO})_2^-$ | 1.7 | 1.0 ± 0.4 | 0.643 ± 0.014 | 2100 ± 80 |
| $\text{Ni}(\text{CO})^-$ | 4.6 | 3.2 ± 0.5 | 1.077 ± 0.013 | 1940 ± 80 |
| Ni^- | 5.4 | 4.1 ± 0.3 | 1.157 ± 0.010 | |

Table 6. Negative ions of $\text{Ni}(\text{CO})_4$ with electron affinity ^[40]

The DEA cross section from Quantemol-N simulations, presented in Fig. 5, have average values of maximum cross section of $1 - 2 \times 10^{-3} \text{Å}^2$ at 0.8eV corresponding to the $\text{Ni}(\text{CO})_3^-$ fragment, representing the curves with electron affinity values between 1.2 to 1.4eV.

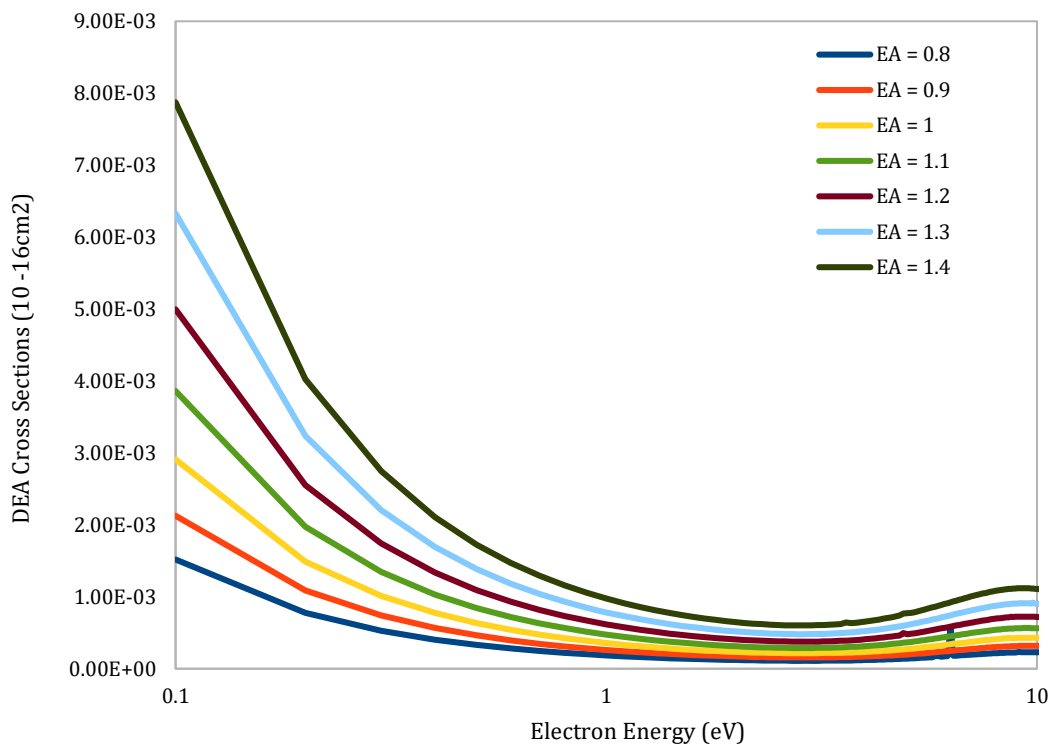


Fig 10. DEA cross sections of Ni(CO)₄

Comparatively, taking into account the fragmentation pattern, the violet (color) spectrum has better accuracy and it is closer to the true value, though all present reliable data within the error limit threshold according to the EA(eV) and vibrational frequency used.

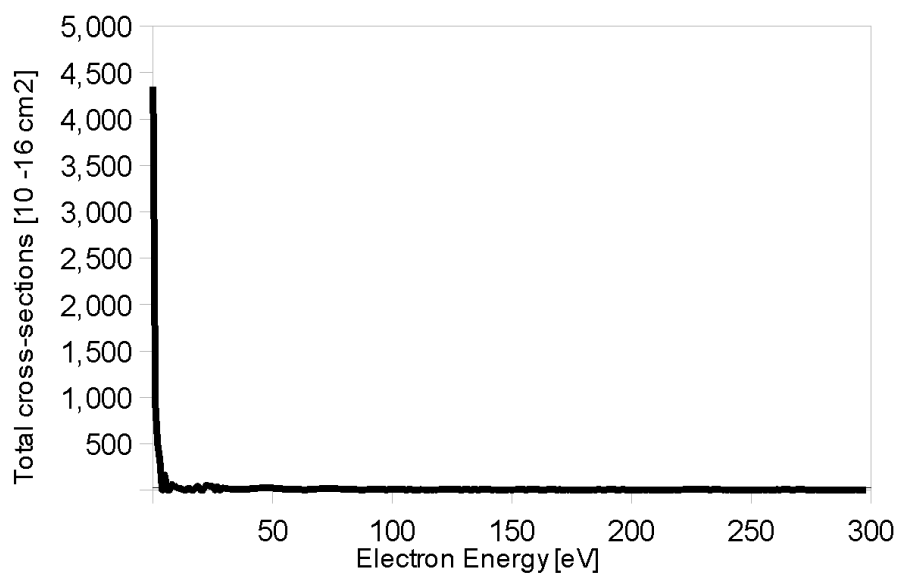


Fig 11. Total cross-sections values for Ni(CO)₄, 1eV to 300eV

With the increase in the electron affinity we have an increase in the cross-section values as seen from Fig. 6 and according to that the viability of the best result. The peaks on the curves with lower electron affinity make the result undesirable, and we could argue that the error comes from applying to the simulation a lower value and not from a real resonance.

The total cross-section from Quantemol-N simulations is in close agreement with the reported literature data for $\sim 100\text{-}300\text{eV}$ of $2 \times 10^{-16}\text{cm}^2$ [47], [48], with a value of $1.6 - 1.8 \times 10^{-16}\text{cm}^2$ in the same energy range. [48] makes reference to the same cross-section value of $2 \times 10^{-16}\text{cm}^2$ in the energy range of $100\text{-}300\text{eV}$ and with the growth of $\text{Ni}_x(\text{CO})_y$ species on $\text{Ag}(111)$ and carbonyl groups spontaneous desorption between $200\text{-}400\text{K}$ resulting pure Ni on the substrate. The total cross-section value is presented in Fig. 8.

Conclusions

With increasing importance to cancer research, materials and superconductors development, nanotechnology and focused electron beam deposition and the scarcity of available data on cross sections, in particular for metal containing compounds, the present article aims to bring an insight into the values of dissociative attachment cross sections obtained through Quantemol-N simulations of the three of the most commonly used compounds, commercially available: $\text{Ni}(\text{CO})_4$, $\text{Co}(\text{CO})_3\text{NO}$ and $\text{Cr}(\text{CO})_6$.

As the use of Quantemol-N simulations would not necessarily replace experimental data, the results show promising use of the software for reliable cross section data that can be utilized in the multitude of the industrial processes requiring an accurate value of these. The approach we employed, based on R-matrix calculations is rather a simple method making use of basic molecular data, structure and symmetry of the molecule, bonds lengths and specificity, all available and easy to obtain from literature or experimental data.

References:

- [1] Huth M., Porrati F., Schwalb C., Winhold M., Sachser R., Dukic M., Adams J., Fantner G., Focused electron beam induced deposition: A perspective, *Beilstein J. Nanotechnol.*, 2012, 3, 597 - 619
- [2] Thorman R.M., Kumar R. T. P., Fairbrother H.D., Ingólfsson O., The role of low-energy electrons in focused electron beam induced deposition: four case studies of representative precursors, *Beilstein J. Nanotechnol.*, 2015, 6, 1904 - 1926

- [3] Van Dorp W.F., Hagen C.W., A critical literature review of focused electron beam induced deposition, *J. Appl. Phys.* 104, 081301, 2008
- [4] Reutt J.E., Wang L.S., Lee Y.T., Shirley D.A., Molecular beam photoelectron spectroscopy of Ni(CO)₄, *Chemical Physics Letters*, Volume 126, number 5, 1986
- [5] McDowell R.S., Horrocks W.D. Jr., Infrared Spectrum of Co(CO)₃NO, J.T. Yates, *J. Chem. Phys.* 34, 530, 1961
- [6] Postler J., Renzler M., Kaiser A., Huber S.E., Probst M., Scheier P., Ellis A.M., Electron-Induced Chemistry of Cobalt Tricarbonyl Nitrosyl (Co(CO)₃NO) in Liquid Helium Nanodroplets, *J. Phys. Chem. C*, 2015, 119, 36, 20917 - 20922
- [7] Engmann S., Stano M., Papp P., Brunger M.J., Matejčik S., Ingólfsson O., Absolute cross sections for dissociative electron attachment and dissociative ionization of cobalt tricarbonyl nitrosyl in the energy range from 0eV to 140eV, *J. Chem. Phys.*, 2013, 138, 044305
- [8] Rosenberg S.G., Barclay M., Fairbrother D.H., Electron Beam Induced Reactions of Adsorbed Cobalt Tricarbonyl Nitrosyl (Co(CO)₃NO) Molecules, *J. Phys. Chem. C*, 2013, 117, 16053 - 16064
- [9] McDowell R.S., Horrocks W.D., Yates J.T., Infrared Spectrum of Co(CO)₃NO, *J. Chem. Phys.*, 1961, 34, 530-534
- [10] Horrocks W.D., Taylor R.C., Infrared Spectroscopic Study of Derivatives of Cobalt Tricarbonyl Nitrosyl, *Inorg. Chem.*, 1963, 2, 723-727
- [11] Junk G.A., Svec H.J., Energetics of the Ionization and Dissociation of Ni(CO)₄, Fe(CO)₅, Cr(CO)₆, Mo(CO)₆ and W(CO)₆, *Zeitschrift für Naturforschung* 23b, 1-9, 1968
- [12] Song M.-Y., Yoon J.-S., Cho H., Itikawa Y., Karwasz G.P., Kokoouline V., Nakamura Y., Tennyson J., Cross Sections for Electron Collisions with Methane, *J. Phys. Chem. Ref. Data* Vol. 44, No. 2, 2015
- [13] Tennyson J., Electron-molecule collision calculations using the R-matrix method, *Physics Reports* 491, 2010, 29-76
- [14] Brigg W.J., Tennyson J., Plummer M., R-matrix calculations of low-energy electron collisions with methane, *J. Phys. B: At. Mol. Opt. Phys.* 47, 2014, 185203
- [15] Munro J.J., Harrison S., Fujimoto M.M., Tennyson J., A dissociative electron attachment cross-sections estimator, *Journal of Physics: Conference Series* 388, 2012, 012013
- [16] Bartz J.A., Friday T.O., Goodman B.R., Kooi S.E., Blair R.G., Polik W.F., Energy Disposal in the Photodissociation of Co(CO)₃NO near 225nm, *Journal of Physical Chemistry A*, Vol.102, No.52, 10697-10702, 1998
- [17] Sawyer K.R., Steele R.P., Glascoe E.A., Cahoon J.F., Schlegel J.P., Head-Gordon M., Harris C.B., Direct Observation of Photoinduced Bent Nitrosyl Excited - State Complexes, *J. Phys. Chem. A* 2008, 112, 8505 – 8514

- [18] Nakata H., Nagamori K., Yamasaki K., Kohguchi H., Detection of direct NO ligand loss in the ultraviolet photodissociation of $\text{Co}(\text{CO})_3\text{NO}$, *Chemical Physics Letters* 707 (2018), 150 -153
- [19] Wagner R.J.V., Henning N., Krüger B.C., Barratt Park G., Altschäffel J., Kandratsenka A., Wodtke A.M., Schäfer T., Vibrational Relaxation of Highly Vibrationally Excited CO Scattered from Au(111): Evidence for CO^- Formation, *J. Phys. Chem. Lett.* 2017, 8, 4887 - 4892
- [20] McKinlay R.G., Almeida N.M.S., Coe J.P., Paterson M.J., Excited States of the Nickel Carbonyls $\text{Ni}(\text{CO})$ and $\text{Ni}(\text{CO})_4$: Challenging Molecules for Electronic Structure Theory, *J. Phys. Chem. A* 2015, 10076 – 10083
- [21] Bamford C.H., Compton R.G., Tipper C.F.H., *Decomposition of Inorganic and Organometallic Compounds*, pp 200, Volume 4, Decomposition of inorganic and organometallic compounds, 1972
- [22] Büker H.H., Maître P., Ohanessian G., Theoretical Study of Tungsten Carbonyl Complexes $\text{W}(\text{CO})_n^+(n=1-6)$: Structures, Binding Energies, and Implications for Gas Phase Reactivities, *J. Phys. Chem. A* 1997, 101, 3966-3976
- [23] Distefano G., Photoionization Study of $\text{Fe}(\text{CO})_5$ and $\text{Ni}(\text{CO})_4$, *Journal of Research of the National Bureau of Standards – A. Physics and Chemistry* Vol. 74A, No. 2, March – April 1970
- [24] Mihaylov M., Hadjiivanov K., Knözinger H., Formation of $\text{Ni}(\text{CO})_4$ during the interaction between CO and silica-supported nickel catalyst: an FTIR spectroscopic study, *Catalysis Letters* Vol. 76, No. 1-2, 2001
- [25] Barnes L.A., Liu B., Lindh R., The Structure and Energetics of $\text{Cr}(\text{CO})_6$, *The Journal of Chemical Physics*, March 1993
- [26] Sherwood D.E., Hall M.B., Theoretical Study of the Dissociation of a Single Carbonyl from Chromium Hexacarbonyl, *Inorg. Chem.* 1983, 22, 93-100
- [32] Turner N.J., Martel A.A., Waller I.M., Electron Affinity of $\text{Co}(\text{CO})_2\text{NO}$ Measured by Negative-Ion Photoelectron Spectroscopy, *J. Phys. Chem.* 1994, 98, 474-477
- [28] Whitaker A., Jefferey J.W., The Crystal Structure of Chromium Hexacarbonyl, *Acta Cryst.* 1967, 23, 977
- [29] Pierloot K., Tsokos E., Vanquickenborne L.G., Optical Spectra of $\text{Ni}(\text{CO})_4$ and $\text{Cr}(\text{CO})_6$ Revisited, *J. Phys. Chem.* 1996, 100, 16545-16550
- [30] Kotzian M., Rösch N., Schröder H., Zerner M.C., Optical Spectra of Transition-Metal Carbonyls: $\text{Cr}(\text{CO})_6$, $\text{Fe}(\text{CO})_5$ and $\text{Ni}(\text{CO})_4$, *J. Am. Chem. Soc.* 1989, 111, 7687-7696
- [31] Vilaume S., Strich A., Daniel C., Perera S.A., Bartlett R.J., A coupled cluster study of the electronic spectroscopy and photochemistry of $\text{Cr}(\text{CO})_6$, *Phys. Chem. Chem. Phys.* 2007, 9, 6115-6122

- [32] Khreis J.M., Ameixa J., Ferreira da Silva F., Denifl S., Interactions of low-energy electrons with the FEBID precursor chromium hexacarbonyl ($\text{Cr}(\text{CO})_6$), *Beilstein J. Nanotechnol.* 2017, 8, 2583-2590
- [33] Pollak C., Rosa A., Baerends E.J., Cr-CO Photodissociation in $\text{Cr}(\text{CO})_6$: Reassessment of the Role of Ligand Field Excited States in the Photochemical Dissociation of Metal - Ligand Bonds, *J. Am. Chem. Soc.* 1997, 119, 7324-7329
- [34] Barnes L.A., Liu B., Lindh R., The Structure and energetics of $\text{Cr}(\text{CO})_6$ and $\text{Cr}(\text{CO})_5$, *J. Chem. Phys.* 1993
- [35] Beach N.A., Gray H. B., Electronic structures of metal hexacarbonyls, *J. Am. Chem. Soc.* 1968, 90, 21, 5713-5721
- [36] Fukuda R., Hayaki S., Nakatsuji H., Valence ionization spectra of group six metal hexacarbonyls studied by the symmetry-adapted cluster-configuration interaction method, *J. Chem. Phys.* 131, 2009, 174303
- [37] Winters R.E., Kiser R.W., Ions Produced by Electron Impact with the Dimetallic Carbonyls of Cobalt and Manganese, *J. Phys. Chem.* 1965, 69, 5, 1618-1622
- [38] Foffani A., Pignataro S., Cantone B., Grasso F., Calculation of Ionization Potentials for Aromatic Compounds, *Z. Physik. Chem., Neue Folge*, 42, 221, 1964
- [39] Kopyra J., Maciejewska P., Maljković J., Dissociative electron attachment to coordination complexes of chromium: chromium(0) hexacarbonyl and benzene-chromium(0) tricarbonyl, *Beilstein J. Nanotechnol.* 2017, 8, 2257-2263
- [40] Stevens A.E., Feigerle C.S., Lineberger W.C., Laser Photoelectron Spectrometry of $\text{Ni}(\text{CO})_n$, $n = 1-3$, *J. Am. Chem. Soc.* 1982, 104, 5026-5031
- [41] Compton R.N., Stockdale J.A.D., Formation of gas - phase negative ions in $\text{Fe}(\text{CO})_5$ and $\text{Ni}(\text{CO})_4$, *Intl. J. of Mass Spectrometry and Ion Physics*, 1976, Vol. 22, Issue 1-2, 47-55
- [42] Yamazaki E., Okabayashi T., Tanimoto M., Detection of free nickel monocarbonyl, NiCO : rotational spectrum and structure, *J. Am. Chem. Soc.* 2004, 126, 1028-1029
- [43] Hedberg L., Iijima T., Hedberg K., Nickel tetracarbonyl, $\text{Ni}(\text{CO})_4$, I. Molecular Structure by gaseous electron diffraction. II. Refinement of quadratic force field, *J. Chem. Phys.* 1979, 70, 3224 - 3229
- [44] Ehlers A.W., Dapprich S., Vyboishchikov S.F., Frenking G., Structure and Bonding of the Transition-Metal Carbonyl Complexes $\text{M}(\text{CO})_5\text{L}$ (M)Cr, Mo, W) and $\text{M}(\text{CO})_3\text{L}$ (M) Ni, Pd, Pt; L) CO, SiO, CS, N₂, NO⁺, CN⁻, NC⁻, HCCH, CCH₂, CH₂, CF₂, H₂), *Organometallics* 1996, 15, 105-117
- [45] Papp P., Engmann S., Kučera M., Stano M., Matejčík Š., Ingólfsson O., An experimental and theoretical study on structural parameters and energetics in ionization and dissociation of cobalt tricarbonyl nitrosyl, *International Journal of Mass Spectrometry* 356 (2013) 24-32

- [46] Braga D., Grepioni F., Orpen G., Ni(CO)₄ and Fe(CO)₅: Molecular Structures in the Solid State, *Organometallics* 1993,12, 1481-1483
- [47] Ramsier R.D., Henderson M.A., Yates Jr. J.T., Electron induced decomposition of Ni(CO)₄ adsorbed on Ag(111), *Surface Science*, Volume 257, Issues 1–3, 1991, Pages 9-21
- [48] Utke I., Melngailis J., Hoffmann P., Gas-assisted focused electron beam and ion beam processing and fabrication, *J. Vac. Sci. Technol. B* 26(4), Jul/Aug 2008
- [49] Fuss W., Schmid W.E., Trushin S.A., Ultrafast Photodissociation Dynamics of Ni(CO)₄, *J. Phys. Chem. A* 2001, 105, 333-339
- [50] Crespo-Otero R., Barbatti M., Cr(CO)₆ photochemistry: Semi-classical study of UV absorption spectral intensities and dynamics of photodissociation, *The Journal of Chemical Physics* 134, 2011, 164305
- [51] Sawyer K. R., One- and two-dimensional infrared spectroscopic studies of solution-phase homogeneous catalysis and spin-forbidden reactions, PhD Dissertation, 2003, University of California, Berkeley
- [52] UKRmol: a low-energy electron- and positron-molecule scattering suite', J Carr et al, *European Physical Journal D* 66 (2012) 58
- [53] RESON: A program for the detection and fitting of Breit-Wigner resonances', J Tennyson & CJ Noble, *Computer Physics Communications* 33 (1984) 421-424

ANNEX 1:

Atomic structure and X, Y, Z configuration of Cr(CO)₆:

| Atom Label | X [Å] | Y [Å] | Z [Å] |
|------------|-------|-------|-------|
| C1 | 1.34 | 1.34 | 0 |
| C2 | -1.34 | -1.34 | 0 |
| C3 | 0 | 0 | 1.9 |
| C4 | -1.34 | 1.34 | 0 |
| C5 | 0 | 0 | 0 |
| C6 | 2.15 | 2.15 | 0 |

| | | | |
|-----|-------|-------|-------|
| Cr7 | -2.15 | -2.15 | 0 |
| O8 | 0 | 0 | 3.04 |
| O9 | -2.15 | 2.15 | 0 |
| O10 | 0 | 0 | -3.04 |
| O11 | 2.15 | -2.15 | 0 |
| O12 | 0 | 0 | -3.04 |
| O13 | 0 | -3.04 | 0 |

Atomic structure and X, Y, Z configuration of $\text{Co}(\text{CO})_3\text{NO}$:

| Atom Label | X [Å] | Y [Å] | Z [Å] |
|------------|-------|-------|-------|
| Co1 | -0.1 | 0 | 0 |
| C2 | 0.66 | -0.81 | -1.4 |
| C3 | 0.66 | -0.81 | 1.4 |
| C4 | 0.66 | 1.62 | 0 |
| O5 | 1.12 | -1.34 | 2.32 |
| O6 | 1.12 | -1.34 | -2.32 |
| O7 | 1.11 | 2.68 | 0 |
| O8 | -2.92 | 0 | 0 |
| N9 | -1.76 | 0 | 0 |

Atomic structure and X, Y, Z configuration of $\text{Ni}(\text{CO})_4$:

| Atom Label | X [Å] | Y [Å] | Z [Å] |
|------------|-------|-------|-------|
| Ni1 | 0 | 0 | 0 |
| C2 | -0.09 | -1.8 | 0.18 |

| | | | |
|----|-------|-------|-------|
| C3 | 1.73 | 0.52 | 0.04 |
| C4 | -0.74 | 0.48 | -1.58 |
| C5 | -0.9 | 0.79 | 1.35 |
| O6 | -0.15 | -2.94 | 0.3 |
| O7 | 2.83 | 0.85 | 0.07 |
| O8 | -1.2 | 0.79 | -2.58 |
| O9 | -1.47 | 1.29 | 2.21 |